A PROPER ORTHOGONAL DECOMPOSITION ANALYSIS OF A REALISTIC LANDING GEAR WITH APPLICATIONS TO NOISE PREDICTION

Paulo R. G. Azevedo Junior, prgajr@gmail.com[1]
William R. Wolf, wolf@fem.unicamp.br[2]

[1]Undergraduate Student, Department of Statistics, 13083-860,University of Campinas.
[2]Assistant Professor, School of Mechanical Engineering, 13083-860, University of Campinas, AIAA Member.

Abstract: *The current paper will present noise predictions of the AIRBUS-ONERA LAGOON landing gear configuration. Numerical simulations of the turbulent flow past the LAGOON landing gear provide the acoustic sources responsible by the noise generation. The Ffowcs Williams & Hawkings (FWH) acoustic analogy formulation is then applied to perform the far-field noise predictions. Proper orthogonal decomposition is employed to extract the most energetic components of the noise sources from the turbulent flow and the noise predictions are accelerated by a 3D wideband fast multipole method. An Optimized Implementation is present in order to achieve maximum performance in terms of processing power and storage optimization. Also a strategy for smooth the Spectra along the time is presented, using the autocorrelation matrix obtained by the Proper orthogonal decomposition.*
Keywords: *Landing Gear, POD, Acoustic Prediction, LAGOON*

1. Introduction

In the past decades, significant jet noise reduction has been achieved due to efforts on the design of more efficient and quieter engines. Since then, airframe noise associated with the unsteady turbulent flow around the aircraft has become a significant source of noise, specially for landing configurations. Therefore, improving prediction techniques for airframe noise generation and propagation is a key topic in aeroacoustics research.

The most significant airframe noise sources at landing configuration are high-lift components and landing gears. Recently, several efforts have been conducted in order to predict noise generation by landing gears. In this context, numerical and experimental studies were performed for simplified and realistic configurations Spalart *et al.* (2011); Sanders *et al.* (2012a). Currently, the American Institute of Aeronautics and Astronautics, AIAA, holds a workshop on Benchmark problems for Airframe Noise Computations, BANC, which fosters the discussion of relevant scientific and technological problems in airframe noise. Among the problems of interest lies the study of the LAGOON landing gear configuration which is analyzed here Manoha and Caruelle (2008, 2009); Deck (2012); Deck *et al.* (2014); Redonnet and Cunha (2014).

With current advances in computational power, turbulent flows over blunt bodies can be numerically resolved with significant accuracy. These unsteady flow simulations provide the noise sources which can then be used to predict the far-field noise. However, this hybrid numerical framework (computational fluid dynamics, CFD, plus computational aeroacoustics, CAA) is still expensive since large computational grids and accurate algorithms are required to capture the most energetic flow scales in the numerical simulations. Furthermore, large datasets need to be computed and stored for the post-processing of the acoustic sources. Accurate aeroacoustic predictions rely on these datasets and adequate statistical post-processing.

The current paper presents noise predictions of the AIRBUS-ONERA LAGOON landing gear configuration. Numerical simulations of the turbulent flow past the LAGOON landing gear provide the acoustic sources responsible by the noise generation. The flow simulation dataset used in the category 8 of the AIAA BANC workshop is employed to compute the acoustic sources. For the present low Mach number flow, only surface data is required for the far-field acoustic predictions which are performed using the Ffowcs Williams & Hawkings (FWH) acoustic analogy Ffowcs Williams and Hawkings (1969). Noise predictions are accelerated by a 3D wideband fast multipole method Wolf (2011); Wolf and Lele (2011b,a). Proper orthogonal decomposition is then employed to extract the most energetic modes composing the noise sources from the turbulent pressure field.

With the present framework, reduced order models can be developed and applied for noise prediction of turbulent flows. The same methodology is employed to predict far-field noise using a porous FWH surface. Results from impermeable and permeable FWH surfaces are compared to experimental measurements and further numerical solutions available in the literature Sanders *et al.* (2012a). An individual assessment of the noise generation by the individual parts (wheels, strut, cavities and main axle) composing the landing gear is presented.

2. Flow Simulation and Acoustic Prediction

Compressible flow simulations of the LAGOON landing gear are performed using detached eddy simulation. Since the interest here is to predict far-field noise at landing configurations, the flow is at a low Mach number, $M_\infty = 0.18$.

More details regarding the numerical methodology can be found in Ref. (AIAA, 2013). Results of the flow simulations are post-processed and unsteady signals of primitive variables are provided along the landing gear surface (here, only pressure fluctuations are needed) and for a cubical permeable FWH surface surrounding the landing gear. After a statistical treatment, these signals are used as an input for the acoustic analogy formulation which provides the far-field noise.

The Ffowcs Williams & Hawkings (FWH) Ffowcs Williams and Hawkings (1969) acoustic analogy formulation is used to predict the acoustic far-field noise radiated by the turbulent flow simulation. The FWH equation is applicable to bodies in arbitrary motion. However, in the present work, noise sources and observer locations are assumed to be in steady uniform motion in a stagnant medium. Following the development by Lockard Lockard (2002), the FWH formulation for steady uniform motion can be written as

$$\left[\hat{p'}H(f)\right] = -\int_{f=0}\left[i\omega\hat{Q}(\vec{y})G(\vec{x},\vec{y}) + \hat{F}_i(\vec{y})\frac{\partial G(\vec{x},\vec{y})}{\partial y_i}\right]dS - \int_{f>0}\hat{T}_{ij}H(f)\frac{\partial^2 G(\vec{x},\vec{y})}{\partial y_i \partial y_j}dV, \tag{1}$$

where p' is the pressure fluctuation, i is the imaginary unit, ω is the angular frequency, $f = 0$ represents the FWH surface and $H(f)$ is the Heaviside function defined as $H(f) = 1$ for $f > 0$ and $H(f) = 0$ for $f < 0$.

Considering a mean flow velocity in the x Cartesian direction, the 3D Green's function that incorporates convective effects Dowling and Ffowcs Williams (1989) is given by

$$G(\vec{x},\vec{y}) = -\frac{e^{-ik\left[\sqrt{(x_1-y_1)^2+(1-M^2)[(x_2-y_2)^2+(x_3-y_3)^2]}-M(x_1-y_1)\right]/(1-M^2)}}{4\pi\sqrt{(x_1-y_1)^2+(1-M^2)\left[(x_2-y_2)^2+(x_3-y_3)^2\right]}}. \tag{2}$$

In Eq. 2, k is the wavenumber, M is the freestream Mach number defined as $M \equiv U_1/c_0$, $\vec{x} = (x_1, x_2, x_3)^t$ is an observer location and $\vec{y} = (y_1, y_2, y_3)^t$ is a source location. The term $\hat{}$ represents a Fourier transformed quantity. The monopole and dipole source terms are

$$Q = \left[\rho\left(u_i + U_i\right) - \rho_0 U_i\right]\partial f/\partial x_i \tag{3}$$

and

$$F_i = \left[p\delta_{ij} - \tau_{ij} + \rho\left(u_i - U_i\right)\left(u_j + U_j\right) + \rho_0 U_i U_j\right]\partial f/\partial x_j, \tag{4}$$

respectively, and T_{ij} is the Lighthill stress tensor or quadrupole source term given by

$$T_{ij} = \rho u_i u_j + (p' - a^2\rho')\delta_{ij} - \tau_{ij}. \tag{5}$$

In Eqs. 3, 4 and 5, u_i is the fluid velocity vector, U_i is the FWH surface velocity, p is the pressure, ρ_0 is the freestream density, ρ' stands for the density perturbation, a is the speed of sound, δ_{ij} is the Kronecker delta and τ_{ij} is the viscous stress tensor.

In the present work, the surface integrations appearing in Eq. 1 are computed along the landing gear surface, including wheels, cavities and axles, or along the cubical surface which is assumed to be permeable. When a solid surface is employed, the monopole source terms, $\hat{Q}$, become steady in time and do not appear in the frequency domain formulation. Again, along the solid surface, the dipole source terms, $\hat{F}_i$, are only computed by $\hat{F}_i = \hat{p'}\, n_i$ since, for the present high Reynolds number flow, viscous stresses are negligible. The term n_i appearing in the source term represents the component of the outward unit normal vector in the i Cartesian direction. The volume integrations of quadrupole sources in Eq. 1 are also neglected since, for low Mach number flows, the noise generated from quadrupole sources, $\hat{T}_{ij}$, are small compared to that radiated by dipole and monopole sources. This hypothesis will be verified through a comparison of the solutions obtained by the solid and porous FWH surfaces. The latter includes the quadrupole effects contained in the cubical surface.

In this work, the surface integrations are performed using a 3D wideband multi-level adaptive fast multipole method (FMM) in order to accelerate the calculations. In the current context, the FMM consists of clustering noise sources from the landing gear and cubical meshes at different spatial lengths in multipole expansions and, then, evaluating their effects at clusters of observer locations well-separated from the noise sources. We define two well-separated clusters as sets of elements (sources and observers) that are circumscribed by spheres and whose centroids are distant from each other by a length of at least four times their radius.

In the FMM-FWH method, a cubical box surrounds a CFD mesh containing noise sources and an acoustic grid containing several observer locations. Then, a recursive algorithm for the refinement of this box is applied in order to form the refinement levels of the multi-level FMM. The general idea consists of refining the box into eight smaller boxes and inspecting the number of sources and observers contained by each of the new boxes. This process continues until the number of elements inside all the boxes is smaller than or equal to a certain prescribed number. This prescribed number of elements per box will define the maximum refinement level in the FMM. Following an oct-tree algorithm, one can define sets of lists containing some specific boxes, such as boxes that share nodes or edges, well-separated boxes at the same level of refinement and others. These lists will help with the computation of multipole and local expansions including their translations and conversions. The authors refer the reader to Refs. (Wolf and Lele, 2011b,a; Wolf, 2011) for a complete description of the 3D wideband FMM.

3. Proper Orthogonal Decomposition

Proper Orthogonal Decomposition (POD) is a method of data-analysis used to obtain a low-dimension approximation of a high-dimensional process; it is also known as Principal Component Analysis (PCA). The POD technique provides a linear approximation of a set of functions that enable an easier characterization of the more complex original input as a sum of weighted basis functions. For practical applications, the decomposition can be carried out using the classical method or the snapshot method.

The fundamental idea of POD is to decompose a set of scalar quantity distributions $S^{(k)} = (S)^{(k)}_{(i,j)}$. Here, $S^{(k)}$ is the k snapshot of the S scalar quantity, for example, pressure or some component of velocity, and the term i, j represents the index of the grid points where the scalar quantity distribution is obtained. The scalar field distribution is decomposed into a set of linear combinations of a M spatial basis functions (ϕ_m), and the corresponding temporal coefficients $c_m^{(k)}$, where $S^{(k)} = \sum_{m=1}^{M} c_m^{(k)} \phi_m$ with the constraint that the basis functions are orthonormal to each other.

The scalar quantities $S^{(k)}$ are reordered into a combination of rows and written in a matrix form as:

$$S = \begin{bmatrix} S^{(1)} \\ S^{(1)} \\ \vdots \\ S^{(K)} \end{bmatrix} = \begin{bmatrix} s^{(1)}_{i=1,j=1} & s^{(1)}_{i=1,j=2} & \cdots & s^{(1)}_{i=1,j=J} & s^{(1)}_{i=2,j=1} & \cdots & s^{(1)}_{i=I,j=J} \\ s^{(2)}_{i=1,j=1} & s^{(2)}_{i=1,j=2} & \cdots & s^{(2)}_{i=1,j=J} & s^{(2)}_{i=2,j=1} & \cdots & s^{(2)}_{i=I,j=J} \\ \vdots & \vdots & & \vdots & \vdots & & \vdots \\ s^{(K)}_{i=1,j=1} & s^{(K)}_{i=1,j=2} & \cdots & s^{(K)}_{i=1,j=J} & s^{(K)}_{i=2,j=1} & \cdots & s^{(K)}_{i=I,j=J} \end{bmatrix}.$$

Here, the terms I, J represent the total number of grid points in the x, y directions of the grid which describes the scalar field and K is the total number of snapshots. The spatial correlation matrix for the scalar field distribution is then defined by $C = \frac{1}{K}(SS^T)$.

The goal of using the POD technique is to find a sequence of orthonormal basis functions representing the most 'energetic structures' in such a way that the following function is minimized

$$\sum_{k=1}^{K} \|S^{(k)} - \sum_{m=1}^{M} c_m^{(k)} \phi_m\|$$

subject to $(\phi_i, \phi_j) = \delta_{ij}$, where $\|.\|$ denotes the L^2 norm. This minimization is obtained solving the eigenvalue problem of correlation matrix C

$$C\beta_m = \lambda_m \beta_m.$$

In the present work, a singular value decomposition (SVD) is applied to obtain the eigenvalues.

4. Aeroacoustic Predictions

The current section presents aeroacoustic results for the LAGOON landing gear configuration. Figure 1 shows the full geometry of the landing gear including its wheels, axle, cavities and strut (a), a view of the mesh along the wheels (b), and the adaptive refinement of the FMM boxes along the landing gear (c). The surface of the landing gear is represented by $\approx$ 200000 surface elements. In Fig. 2, one can see an exploded view of the individual parts of the landing gear. Experiments and numerical simulations were conducted by several authors and a dataset is provided in the literature by Sanders *et al.* Sanders *et al.* (2012b). In this work, we present results for the same positions of far-field microphones and pressure probes as in Ref. Sanders *et al.* (2012b).

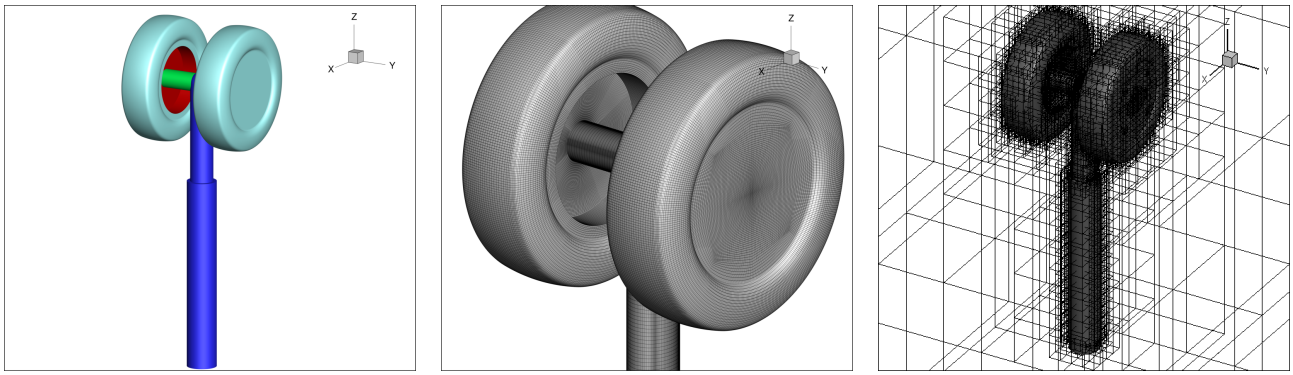

(a) Full view. (b) Mesh detail. (c) Fast multipole method adaptive refinement.

Figura 1: LAGOON landing gear.

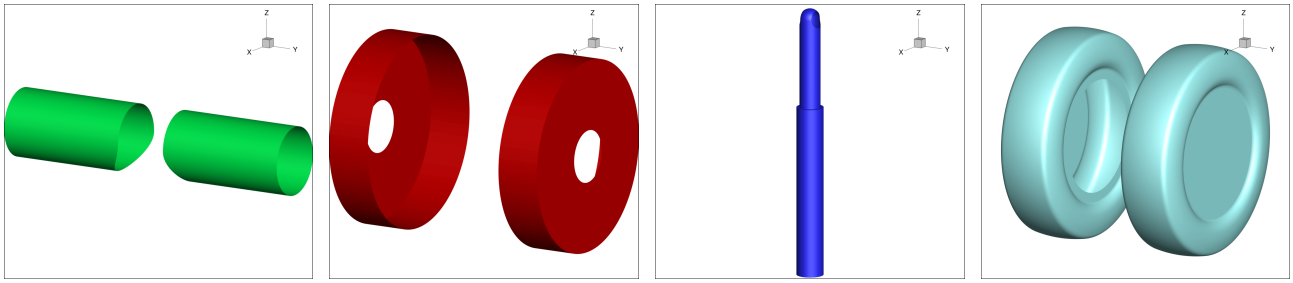

(a) Axle. (b) Rim. (c) Strut. (d) Wheels.

Figura 2: Exploded view of the landing gear.

4.1 Solid Surface

The present section presents results of the FWH formulation implemented for a solid FWH surface. In Fig. 3, plots of power spectral density of surface pressure are shown for two near-field positions (probe locations K1 and K20 of Ref. Sanders *et al.* (2012b)). In the plots, the terms C19 and F2 represent experimental data from different wind tunnel test campaigns. The term numerical represents data obtained from a detached numerical simulation, DES, also available in Ref. Sanders *et al.* (2012b). One can see that the comparison of PSD spectra among different experiments is in reasonable agreement as well as the comparison between the numerical simulations. However, numerical simulations have a hard time resolving the small turbulent scales since DES is well-suited for larger separated flow scales. In this matter, the low frequency content of the spectra shows a good comparison. The terms Probe K1 and K20 represent the current post-processed results which are obtained by an average of 7 bins with 4096 time samples and 50% overlap. For each bin, the fluctuations are computed and windowed.

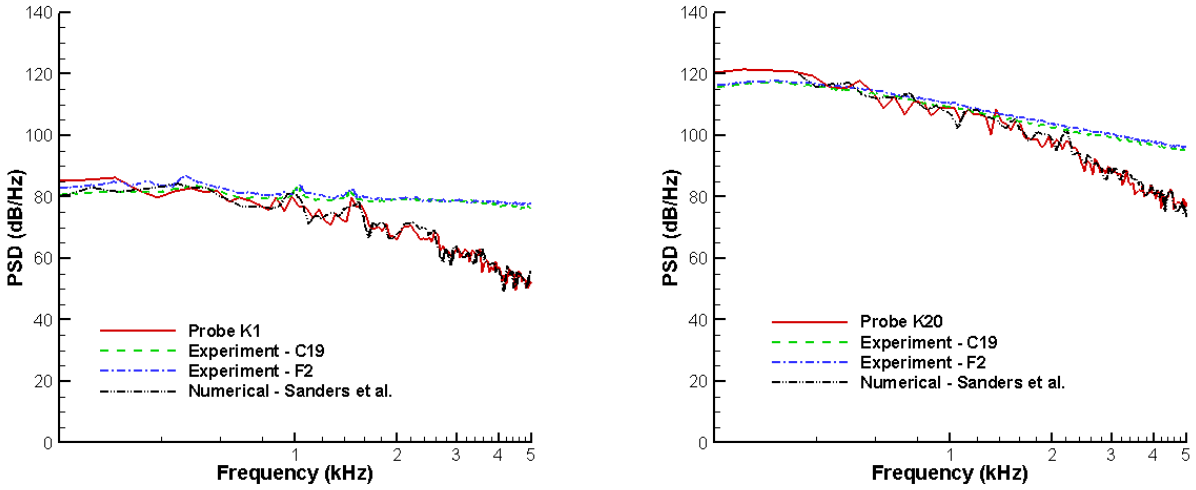

(a) Probe K1. (b) Probe K20.

Figura 3: Comparison of near-field pressure results between experiments and numerical simulations.

Figure 4 also presents plots of PSD, now measured at the far-field microphone locations M3, corresponding to sideline and flyover positions in Ref. Sanders *et al.* (2012b). In this figure, it is possible to compare the far-field noise prediction from experiment and numerical simulation. A good agreement is observed among the PSD plots although the numerical predictions show a closer match for all frequencies. The present plots show the results of the averaged spectra. To perform the far-field noise prediction, the finite-difference grid is transformed in a finite volume grid with a connectivity table. Then, results of surface pressure are Fourier transformed and associated to each independent surface of the finite volume grid. Finally, the FWH equation is applied to radiate the far-field noise.

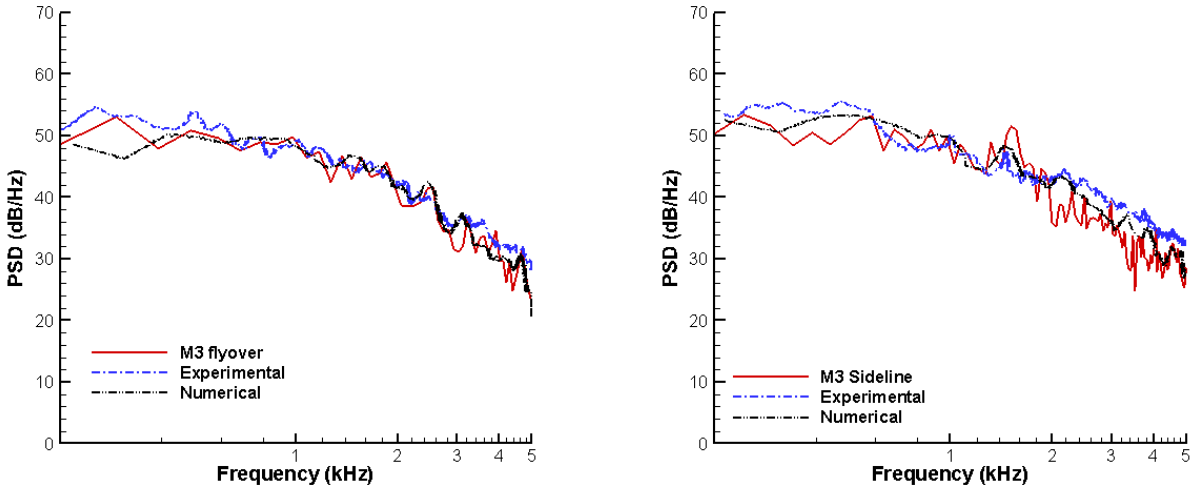

(a) Microphone M3 flyover.

(b) Microphone M3 sideline.

Figura 4: Comparison of far-field acoustic pressure results between experiments and numerical simulation.

Once a good comparison is obtained among acoustic radiation results, we want to perform an assessment of the individual noise sources in the landing gear. Therefore, the FWH equation is applied to the individual surfaces of the axle, wheels, rim and strut. Figure 5 shows the far-field pressure spectra obtained for each of these configurations. One can see that, at low frequencies, the axle, wheels and rim are responsible for the major portion of the far-field noise radiation. At high frequencies, the rims are the major noise sources followed by the axle. The strut does not contribute to the far-field prediction at the present microphones since lift fluctuations should occur in the transverse direction and the dipolar radiation should be minimal in the current observer position.

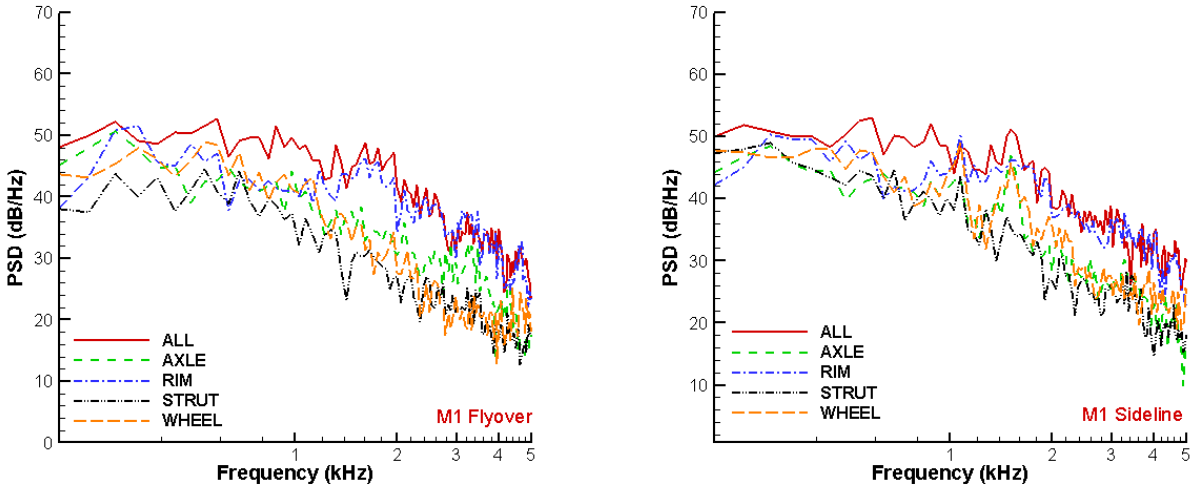

(a) Microphone M1 flyover.

(b) Microphone M1 sideline.

Figura 5: Comparison of the individual noise sources in the landing gear.

In the present work, we apply POD to reconstruct the scattered pressure field along the landing gear surface and, then, we compute the far-field noise using the reconstructed pressure signal. In Fig. 6 (a), one can observe a plot showing the normalized energy of the POD modes for the near-field pressure signal. Here, we are using the entire signal (16384 snapshots) to perform POD, which means that 16384 modes build the complete signal. From the figure, it is possible to see that the first mode has 7% of the total energy of the signal. Horizontal lines show the energy bands of the signal, *i.e.,* the modes that are above 5%, 1% and 0.1% of the total energy. For example, only two modes have more than 5% of the total energy and 150 modes have more than 0.1% of the total energy. In the plot, we see that the first 200 modes contain almost the entire energy of the signal. Figure 6 (b) shows the values of the correlation matrix, which is formed to resolve the POD of the system.

Different norms are employed for POD reconstruction of turbulent flows and if the flow is incompressible, a norm based on the kinetic energy is used to minimize the error. Different norms can be applied to compressible turbulent flows reconstructed using POD. The authors suggest the work from Ref. **?** for a discussion on the topic. In the present work,

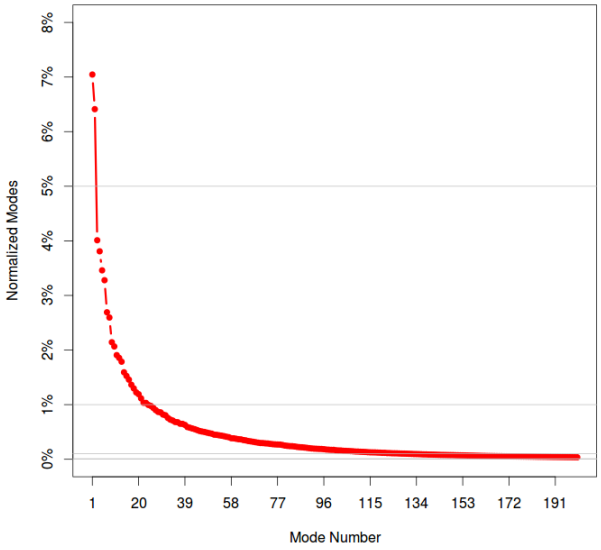

(a) Normalized energy of the POD modes.

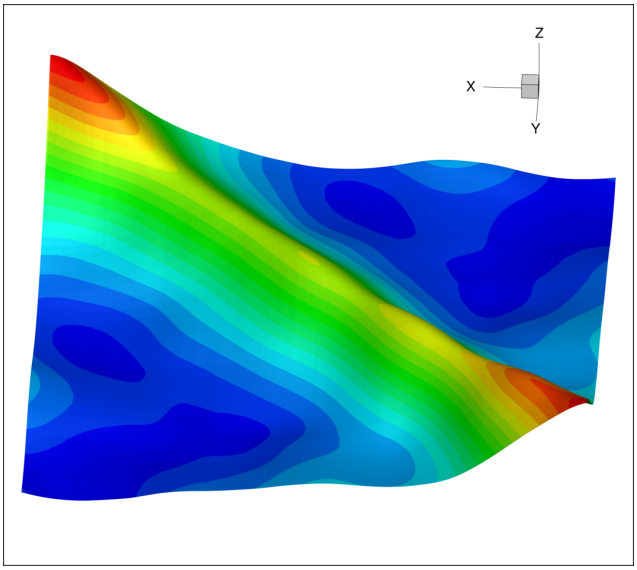

(b) 3D visualization of the correlation matrix.

Figura 6: Application of POD to the near-field pressure signal.

the POD reconstruction is implemented using the values of surface pressure, since only this variable is used in the source reconstruction. Figure 7 presents the results of the POD reconstruction of the turbulent signal along the landing gear surface. One can observe that the pressure signal is recovered inside the rims using the first 30 modes. The strut signal is recovered using the first 60 modes. The small scale structures along the wheel surface are recovered using the first 150 modes.

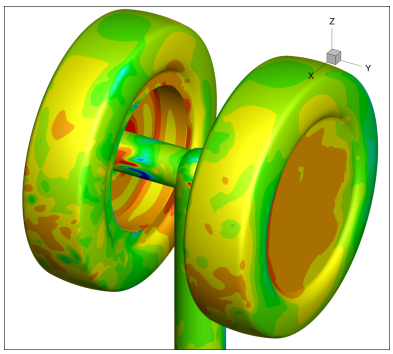

(a) Snapshot of the original pressure signal.

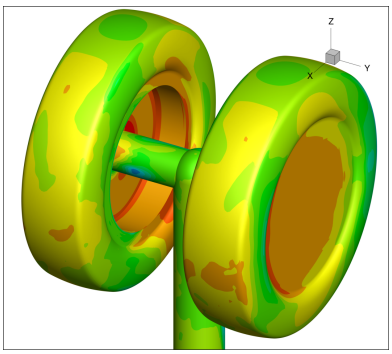

(b) POD reconstruction using the first 5 modes.

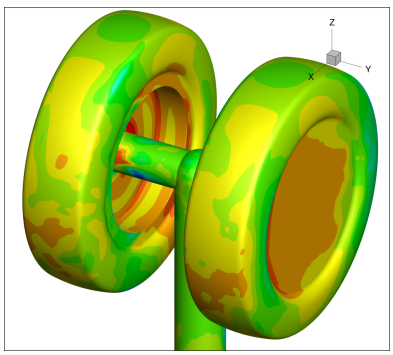

(c) POD reconstruction using the first 30 modes.

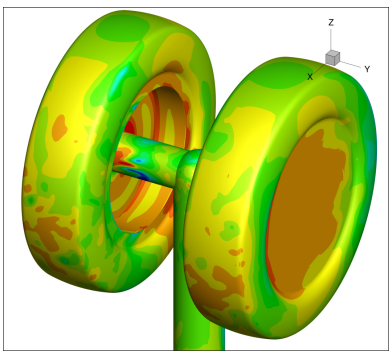

(d) POD reconstruction using the first 60 modes.

Figura 7: POD reconstruction of the turbulent pressure signal along the landing gear surface.

Figure 8 (a) shows the PSD of surface pressure after POD reconstruction. The signal is formed using the modes above 5%, 1% and 0.001% of the energy. This means that the first signal includes the first 2 modes, the second signal has the first 25 modes and the third signal is composed by the first 150 modes. The second signal is able to capture the low-frequency content of the spectrum due to the large scale time fluctuations and the signal with 150 modes shows an excellent agreement with the original turbulent signal, except at the highest frequencies. The far-field acoustic pressure spectra of the reconstructed signal for microphone M3 at flyover is shown in Fig. 8 (b). Using 150 modes, the far-field noise is predicted with accuracy, except for the high-frequency content, which depends on the capture of the fine turbulent scales.

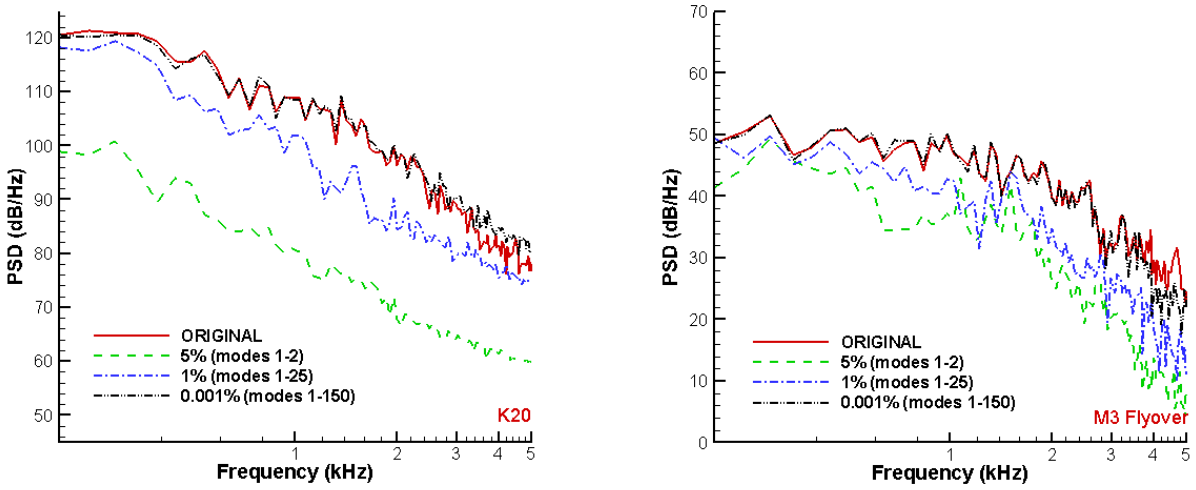

(a) Probe K20 signal reconstruction using POD.

(b) Far-field spectra of reconstructed signal for microphone M3 at flyover.

Figura 8: POD reconstructed spectra.

5. Conclusions

The current paper presents noise predictions of the AIRBUS-ONERA LAGOON landing gear configuration. Acoustic predictions are obtained by the Ffowcs Williams & Hawkings (FWH) acoustic analogy formulation. Results of far-field predictions are performed using the pressure fluctuations along the landing gear surface, obtained from compressible detached eddy simulation. Proper orthogonal decomposition is employed to reconstruct the turbulent flow and far-field predictions from the reconstructed signals show excellent agreement to those computed by the original signal.

6. Acknowledgements

The authors acknowledge the financial support received from Fundação de Amparo à Pesquisa do Estado de São Paulo, FAPESP, under Grant No. 2013/03413-4 and from Conselho Nacional de Desenvolvimento Científico e Tecnológico, CNPq, under Grant No. 470695/2013-7. The authors also acknowledge FAPESP por providing a scholarship to the first author, Grant No. 2014/22202-7. The computational resources provided by CENAPAD-SP under Project No. 551 are also acknowledged. The LAGOON database is owned by ONERA and AIRBUS and it was provided to the authors by ONERA under permission by AIRBUS in the framework of the AIAA-BANC Workshop. The authors thank Stéphane Redonnet, David Lockard and Leonard Lopes for the help handling the data and the discussion along this work. AIAA (2013) Lockard (2002)

7. REFERENCES

AIAA, 2013. "Third aiaa workshop on benchmark problems for airframe noise computations". 31 Oct. 2013 <https://info.aiaa.org/tac/ASG/FDTC/DG/BECAN_files_/BANCIII.htm>.

Deck, S., 2012. "Recent improvements in the zonal detached eddy simulation (ZDES) formulation". *Theoretical and Computational Fluid Dynamics*, Vol. 26, No. 6, pp. 523–550.

Deck, S., Gand, F., Brunet, V. and Ben Khelil, S., 2014. "High-fidelity simulations of unsteady civil aircraft aerodynamics: stakes and perspectives. application of zonal detached eddy simulation". *Philosophical Transactions of the Royal Society of London A: Mathematical, Physical and Engineering Sciences*, Vol. 372, No. 2022.

Dowling, A.P. and Ffowcs Williams, J.E., 1989. *Sound and Sources of Sound*. Horwood Publishing, Westergate.

Ffowcs Williams, J.E. and Hawkings, D.L., 1969. "Sound generation by turbulence and surfaces in arbitrary motion". *Royal Society of London Philosophical Transactions Series A*, Vol. 264, pp. 321–342.

Lockard, D.P., 2002. "A comparison of ffowcs williams-hawkings solvers for airframe noise applications". In *Proceedings of the 8th AIAA/CEAS Aeroacoustics Conference*. Breckenridge, CO.

Manoha, E., B.J. and Caruelle, B., 2008. "LAGOON: an experimental database for the validation of CFD/CAA methods for landing gear noise predition". In *Proceedings of the 14th AIAA/CEAS Aeroacoustics Conference*. Vancouver, Canada.

Manoha, E., B.J.C.V. and Caruelle, B., 2009. "LAGOON: further analysis of aerodynamic experiments and early aeroacoustics results". In *Proceedings of the 19th AIAA/CEAS Aeroacoustics Conference*. Miami, FL.

Redonnet, S. and Cunha, G., 2014. "Variations on the same BANC category 8 theme: towards the development of a high fidelity acoustic hybrid method using computational aeroacoustics". In *Proceedings of the 20th AIAA/CEAS Aeroacoustics Conference*. Atlanta, GA.

Sanders, L., Manoha, E., Ben-Khelil, S. and Fracois, C., 2012a. "Lagoon : new Mach landing gear noise computation and further analysis of the CAA process". In *Proceedings of the 18th AIAA/CEAS Aeroacoustics Conference*. Colorado Springs, CO.

Sanders, L., Manoha, E., Ben Khelil, S. and François, 2012b. "Lagoon : New mach landing gear noise computation and further analysis of the caa process". In *Proceedings of the 18th AIAA/CEAS Aeroacoustics Conference*. Colorado Springs, CO.

Spalart, P.R., Shur, M.L., Strelets, M.K. and Travin, A.K., 2011. "Initial noise predictions for rudimentary landing gear". *Journal of Sound and Vibration*, Vol. 330, pp. 4180–4195.

Wolf, W.R., 2011. *Airfoil aeroacoustics, LES and acoustic analogy predictions*. Ph.D. thesis, Stanford University, Stanford.

Wolf, W.R. and Lele, S.K., 2011a. "Aeroacoustic integrals accelerated by fast multipole method". *AIAA Journal*, Vol. 49, pp. 1466–1477.

Wolf, W.R. and Lele, S.K., 2011b. "Wideband fast multipole boundary element method: application to acoustic scattering from aerodynamic bodies". *International Journal for Numerical Methods in Fluids*, Vol. 67, pp. 2108–2129.